3D DEM Evaluation of Aggregate Shear Bands and Geogrid Deformations in Pullout Tests

Conference Paper · January 2025

CITATIONS
0

READS
45

3 authors, including:

Yafei Jia
Wuhan University
16 PUBLICATIONS **83** CITATIONS
SEE PROFILE

Yewei Zheng
Wuhan University
80 PUBLICATIONS **689** CITATIONS
SEE PROFILE

3D DEM Evaluation of Aggregate Shear Bands and Geogrid Deformations in Pullout Tests

Yafei Jia[1, 2], Jorge G. Zornberg, F.ASCE[3], and Yewei Zheng[4], Ph.D., A.M.ASCE

[1]School of Civil Engineering, Wuhan University, Wuhan, Hubei 430072, China; Email: yafeijia@whu.edu.cn
[2]Department of Civil, Architectural, and Environmental Engineering, University of Texas at Austin, Austin, TX 78712. Email: yafeijia@utexas.edu
[3]Department of Civil, Architectural, and Environmental Engineering, University of Texas at Austin, Austin, TX 78712. Email: zornberg@mail.utexas.edu
[4]School of Civil Engineering, Wuhan University, Wuhan, Hubei 430072, China; Email: yzheng@whu.edu.cn

ABSTRACT

Pullout tests are commonly used to investigate geogrid-aggregate interaction. Shear band formation can provide relevant insight into understanding load mobilization and failure of geogrid-aggregate interfaces. In this study, pullout test results of geogrids embedded in aggregates were experimentally generated and subsequently simulated to investigate shear band development in the aggregate material and geogrid deformation. A three-dimensional (3D) Discrete Element Method (DEM) model was carefully calibrated using the experimental results. The 3D deformation behavior of the geogrid and shear behavior of aggregates with complex particle shapes were successfully reproduced. The analysis of the particle displacement distribution indicates that the shear bands exhibit varying thicknesses above and below the geogrid reinforcement plane. Visualization of the 3D deformation of the geogrid reveals that the associated bending deformation of the transverse ribs leads to an increase in local stresses and strains at the edges of the longitudinal ribs. Conversely, smaller strains are observed in the middle of the longitudinal ribs.

INTRODUCTION

Geogrids are used extensively in many geotechnical and transportation applications, including reinforced soil walls, paved and unpaved roads, and railway ballast (Indraratna et al., 2013; Jewell et al., 1985; Zornberg et al., 2000). The effective load transfer through interaction between the geogrid and surrounding soil or aggregate material is crucial to enhancing the mechanical behavior of the soil-geogrid composite. Pullout tests are a widely adopted experimental method to evaluate the soil-geogrid interaction behavior and determine the pullout resistance.

The pullout resistance is governed by several factors, including the properties of the geogrid (e.g., geometry, stiffness, aperture size), characteristics of the aggregate (e.g., particle size and shape, gradation, density), and applied normal stresses (Moraci and Recalcati, 2006). The formation and development of shear bands within the aggregate mass may provide significant insight into the pullout process. Shear bands are zones of intense shear deformation that develop due to strain localization within soil or granular materials subjected to shear loading (Jewell, 1990). The formation and propagation of shear bands play a key role in the mobilization of pullout resistance and the overall behavior of the geogrid-aggregate system. Understanding the mechanisms governing shear band formation and interaction with geogrid reinforcement may prove particularly useful for optimizing the design of reinforced soil structures.

Experimental studies have provided valuable insight into pullout behavior and the development of shear bands (Peng and Zornberg, 2019; Zhou et al., 2012). However, experimental methods have inherent limitations in capturing the internal deformation mechanisms, shear band formation, and the three-dimensional (3D) nature of geogrid deformation. Traditional measurement techniques, such as displacement transducers and strain gauges, can only provide localized measurements at discrete points, making it challenging to comprehensively understand the overall deformation field and shear band evolution. In recent years, the Discrete Element Method (DEM) has emerged as a powerful numerical tool for simulating the behavior of granular materials and their interaction with a geosynthetic reinforcement (Ferellec and McDowell, 2012; Jia et al., 2023; Wang et al., 2024). In DEM models, the aggregate is treated as an assembly of discrete particles that interact through contact forces, facilitating the explicit modeling of particle-scale mechanisms and simulation of complex deformation patterns (Ferellec and McDowell, 2010). By incorporating the appropriate contact models and calibrating the DEM model parameters using experimental data, DEM simulations can capture the realistic behavior of aggregate materials, including the formation and propagation of shear bands. Furthermore, DEM simulations can provide detailed data on the particle-scale deformation field, enabling the visualization and quantification of shear band characteristics that are difficult to obtain through experimental means alone.

Aiming at contributing to a deeper understanding of the mechanisms governing soil-geogrid interaction, this study investigated shear band formation and geogrid deformation during pullout tests through a combination of experimental testing and 3D DEM simulations. The experimental results were used to calibrate the DEM model, facilitating accurate representations of the 3D geogrid deformation, complex particle shapes and geogrid-aggregate interaction. The insight gained from this research could inform the optimization of geogrid products and the improvement of design methodologies for reinforced soil structures.

EXPERIMENTS AND DEM SIMULATION

Geogrid. A biaxial polypropylene geogrid with a 65-mm aperture size was selected for this study. The DEM model captured the geogrid geometry by using bonded spherical particles of varying diameters (1.5 – 3 mm) arranged in a gridded pattern to represent the actual aperture shapes and

cross-sectional thickness variations of the ribs. The linear parallel bond contact model (Potyondy and Cundall, 2004) was employed to simulate the axial force transfer, bending moments and torsional resistance between bonded particles. The effective bond modulus, $\overline{E}^*$, of the linear parallel bond model is defined as a segmented linear function of local strain to achieve a nonlinear response in tensile behavior, as follows:

$$\overline{E}^* = \overline{k}_n L = \begin{cases} \lambda_1 \overline{E}_{ini} & (0 < \varepsilon_l \le 2\%) \\ \lambda_2 \overline{E}_{ini} & (2\% < \varepsilon_l \le 5\%) \\ \lambda_3 \overline{E}_{ini} & (5\% < \varepsilon_l) \end{cases} \tag{1}$$

$$\varepsilon_l = \frac{D - L}{L} \times 100\% \tag{2}$$

where λ is a softening coefficient; E_{ini} is the initial bond effective modulus (tension only) of the geogrid ribs; D is the center distance between two particles in contact; and $L = R_1 + R_2$ is the contact length, which can be represented as the sum of the radius of two pieces in contact. The softening coefficients for the three stages are as follows: $\lambda_1 = 1.0$ for the first stage ($0 < \varepsilon_l \le 2\%$), $\lambda_2 = 0.7$ for the second stage ($2\% < \varepsilon_l \le 5\%$), and $\lambda_3 = 0.7$ for the third stage ($5\% < \varepsilon_l$).

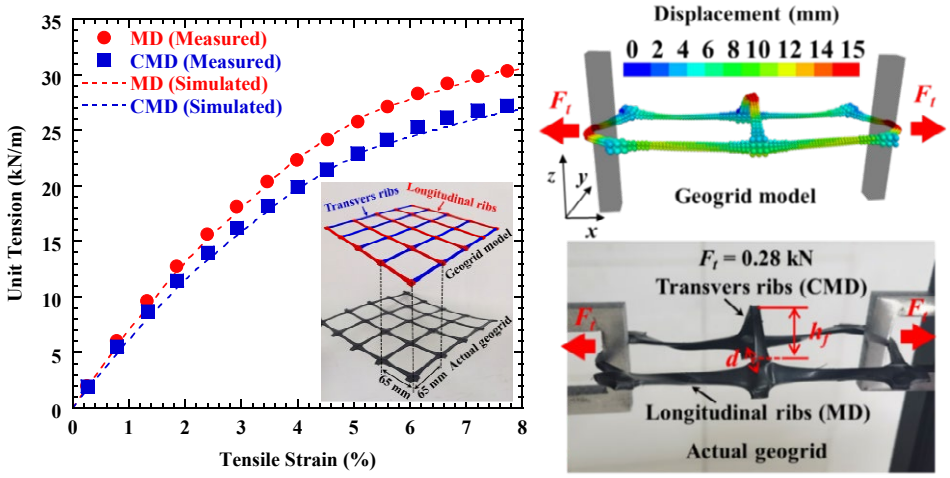

(a) **(b)**

Figure 1. Comparison between experimental results and DEM predictions: (a) tensile test results; and (b) two-aperture extension tests (numerical results and experimental setup).

Figure 1(a) shows the results of rib tension tests. The good comparison between the measured and simulated unit tension-strain responses validates the DEM model's predictions of the in-plane axial stiffness behavior in the Machine Direction (MD) and Cross-Machine Direction (CMD). Additional calibration was accomplished by comparing the out-of-plane deformations obtained experimentally in a two-aperture extension test and numerical predictions of the transverse rib displacements (Figure 1[b]). When reaching a tensile force, F_t, of 0.28-kN, the upward curling of the central transverse rib stabilized, with the maximum vertical displacements (normalized by the junction spacing) obtained in the simulation (0.28) matching well the experimental result (0.30). The final calibrated model successfully captured both the in-plane and

out-of-plane deformations such as longitudinal rib rotations. Overall, the results of tensile and out-of-plane tests illustrate the effectiveness of the DEM model in realistically reproducing the intricate deformation mechanisms of biaxial geogrids.

Aggregates. The aggregates used in the experiments, and adopted in the simulations, consisted of clean angular gravel particles with a mean particle size D_{50} = 16.8 mm, as shown in Figure 2(a). In the DEM simulations, irregularly shaped particles called "clumps" were generated by overlapping multiple spheres of different radii based on polyhedral surfaces representing the actual aggregates (Figure 2[b]). The shear strength envelopes from DEM simulations, obtained using different volume errors for the clump shapes, were calibrated against experimental direct shear test results, as depicted in Figure 2(b). Volume error, E_V, represents the percentage difference between the simulated particle volume and the actual particle volume, relative to the actual particle volume. Higher particle angularity from lower E_V values was found to lead to increased shear strength values, while smoother clump surfaces from higher E_V values underpredicted the shear resistance compared to the experimental data. To balance computational efficiency and accuracy, E_V = 0.087 (E_{V3}) was determined as the optimal value for subsequent simulations. Aggregate particle interaction was simulated using a linear contact model. The particle generation process and parameters were adopted based on the recommendations from the study by Jia et al. (2024).

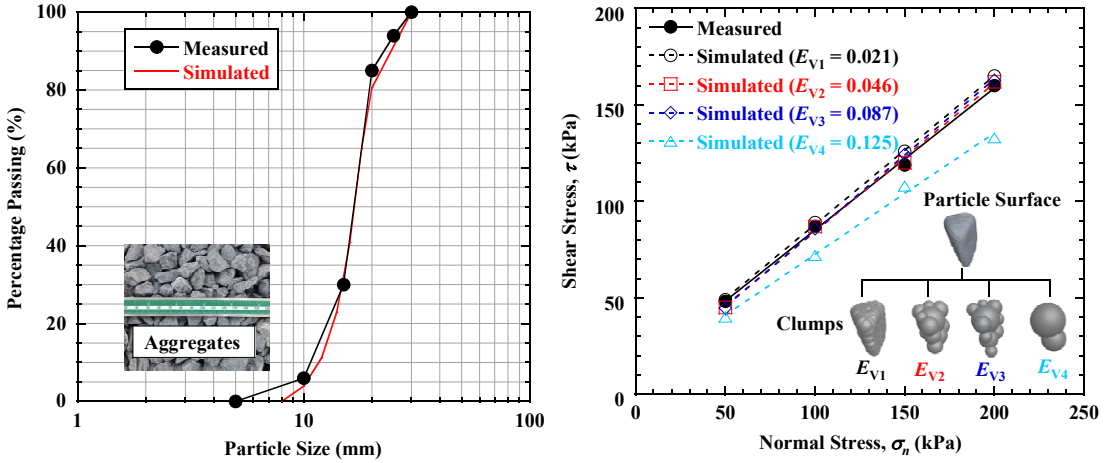

(a) **(b)**

Figure 2. Particles in DEM simulations: (a) particle size distribution; and (b) shear strength envelopes corresponding to different particle shapes (Source: Jia et al., 2024).

DEM Modeling of Pullout Tests. The pullout box presented in Figure 3(a) consists of a rigid steel box with interior dimensions of 300 mm × 300 mm × 400 mm (length × width × height). The front wall has a 10-mm-high opening for clamping and pullout of the geogrid specimen. Transverse ribs near the box edge were trimmed to minimize obstruction during pullout, as suggested by Stahl et al. (2014). A normal (vertical) load was applied to the top of the box using an actuator to maintain a constant normal stress. A clamp securing the geogrid specimen was connected to a horizontal actuator that applied a constant pullout displacement rate. The longitudinal and transverse ribs

were oriented parallel and perpendicular to the pullout direction, respectively. The specific gravity (G_s) of the aggregates is 2.65. A target dry density of 1600.5 kg/m^3 was selected during specimen preparation. A constant pullout rate of 1 mm/min was applied until a 45-mm pullout displacement was reached. Tests were performed under normal stresses of 12.5 kPa, 25 kPa, and 50 kPa, which were selected to represent typical working stress conditions at the aggregate-geogrid interface.

The DEM model (Figure 3[b]) incorporated key features of the experimental setup. The pullout box boundaries were modeled as rigid walls with dimensions identical to the experimental setup. Aggregate particles were generated inside the box using a gravitational field of 9.8 m/s^2 to match the target initial density. A portion of the geogrid extended beyond the front wall, with longitudinal ribs parallel to the pullout direction. The pullout tests were simulated by applying a constant displacement rate to the clamped geogrid section, consistent with the pullout rate used in the experiment.

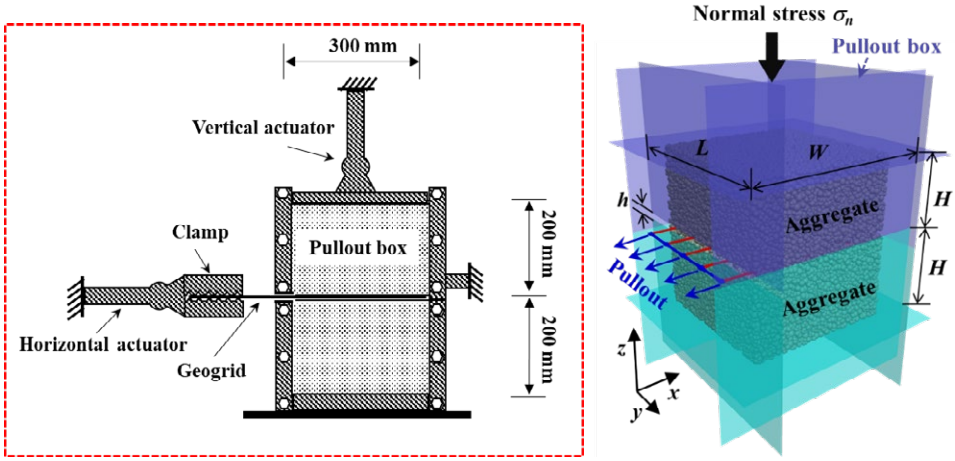

(a) (b)

Figure 3. Pullout test setup: (a) general layout of the pullout box; and (b) DEM pullout test model.

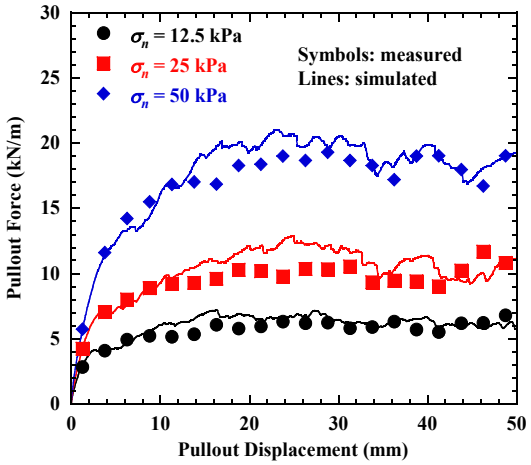

Figure 4. Comparison between experimental results and DEM simulations for geogrids during pullout testing.

The linear contact model (Cundall and Strack, 1979) was employed to simulate the interaction between the geogrid and aggregate particles. Figure 4 presents a comparison between the experimental pullout test results and DEM simulations. Overall, the DEM simulations aligned well with the measured data for all normal stress levels, indicating that the DEM model developed herein accurately captured the development of pullout force with increasing displacement. The input parameters developed for the geogrid, aggregate and geogrid-aggregate interface are summarized in Table 1.

Table 1. Input parameters used in DEM simulations.

Category	Geogrid	Aggregate	Interface
Density, ρ (kg/m^3)	972	2650	/
Local damping coefficient, d	0.7	0.7	/
Frictional coefficient, μ	0.44	0.55	0.44
Effective modulus, E^* (MPa)	3.52×10^4	2×10^3	1.5×10^3
Normal-to-shear stiffness ratio, κ^*	1	1	1
Bond effective modulus (MD), $\overline{E}_{ini}$ (Mpa)	4×10^4	/	/
Bond effective modulus (CMD), $\overline{E}_{ini}$ (Mpa)	3.52×10^4	/	/
Bond normal-to-shear stiffness ratio, $\overline{\kappa}^*$	1×10^2	/	/
Bond gap, $\overline{g}$ (m)	0.75×10^{-3}	/	/

RESULTS AND DISCUSSION

Shear Band. Figure 5 shows the average horizontal displacement distribution of particles at different pullout frontal displacements (negative values correspond to displacements in the pullout direction). The average horizontal particle displacement increased with pullout frontal displacement (δ_p). Maximum particle displacement at each pullout frontal displacement increment occurred at the elevation of the geogrid and decreased with increasing distance from this elevation. This displacement pattern reflects the strain localization trend during the pullout mobilization. Shear bands, which are zones of intense shear deformation, develop due to strain localization within the aggregates. The gradient of particle displacements along the pullout direction can be used to determine the thickness of these shear bands (Jing et al., 2018). For example, at a pullout frontal displacement of δ_p = 48 mm, the thickness corresponding to shear bands both above and below the geogrid, was determined to be $5.7D_{50}$. The upper shear band thickness was 57.1 mm ($3.4D_{50}$), while the lower shear band thickness was 38.6 mm ($2.3D_{50}$). The upper shear band was slightly thicker than the lower one. This difference can be attributed to potential upward particle movement and dilation at the geogrid-aggregate interface under shear, resulting in a thicker shear band above the geogrid.

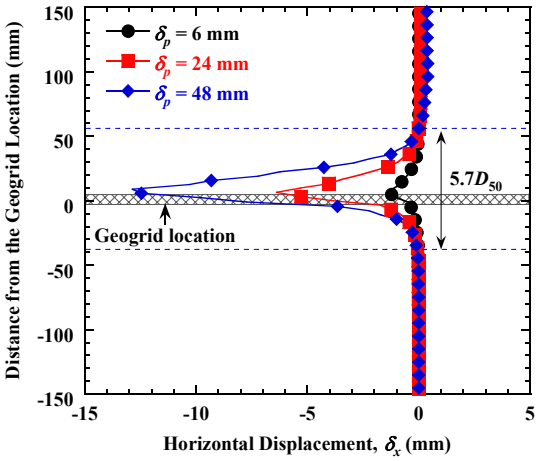

Figure 5. Average horizontal displacement distribution of particles.

Geogrid Deformation. The polypropylene geogrid used herein falls in the general category of extensible reinforcement materials. Figure 6(a) shows the strain profiles, for increasing pullout frontal displacements, in the middle of the longitudinal ribs while Figure 6(b) displays the strain distribution at one of the edges of the longitudinal ribs. It can be observed that tensile strains increased with increasing pullout frontal displacement, δ_p. The strain profiles exhibit a general decrease along the longitudinal rib length, showing significant strain fluctuations at the junction where transverse and longitudinal ribs intersect. The observed behavior can be attributed to the bending deformation of the transverse ribs due to passive resistance mechanisms. Figure 6 also presents tensile force and deformation distributions for a typical geogrid aperture, where significant bending deformation of the transverse ribs can be observed. Near the junctions, the significant bending deformation of the transverse led to localized stress and strain increases at the edge of the longitudinal ribs, while smaller strains occurred in the middle of the longitudinal ribs.

Figure 7 shows the average axial tensile strain distribution along the longitudinal ribs of the geogrid calculated using the junction displacements. The average axial tensile strains decrease from a maximum value at the loading end to zero at the embedded end, aligning with the localized strain distribution shown in Figure 6. Figure 7 also displays the rotation of the geogrid ribs relative to their initial state to reflect the overall geogrid deformation as pullout displacement increased. The transverse ribs closest to the applied frontal load show more pronounced bending deflections, with this trend becoming more prominent with increasing pullout frontal displacement.

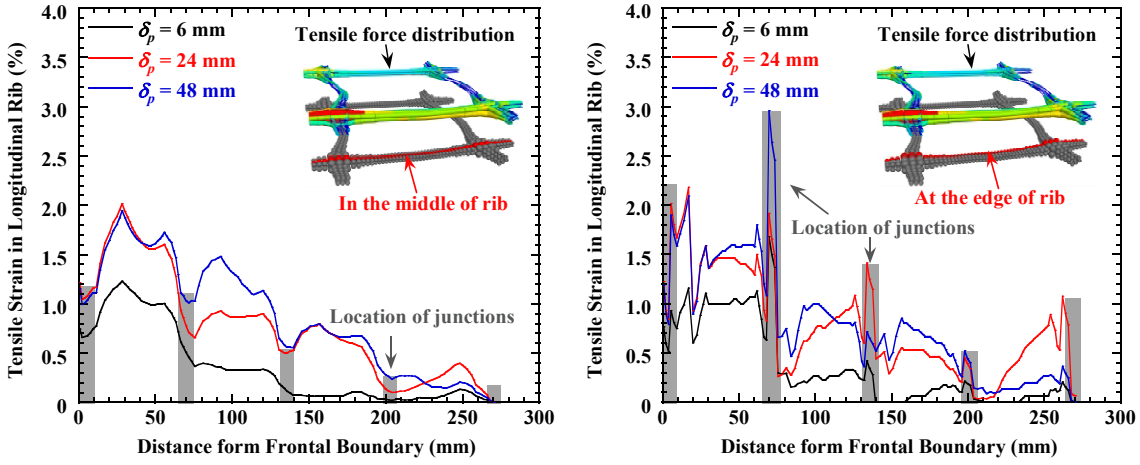

Figure 6. Tensile strains in longitudinal geogrid ribs: (a) strain at the middle of ribs; and (b) strain at the edge of ribs.

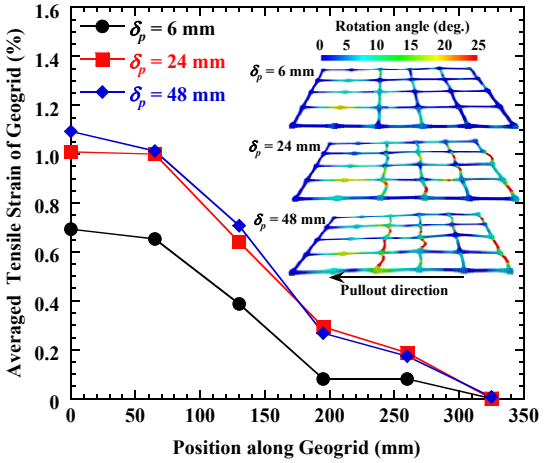

Figure 7. Distributions of average tensile strain along longitudinal ribs.

CONCLUSIONS

In this study, three-dimensional (3D) Discrete Element Method (DEM) analyses were conducted to simulate pullout tests of geogrids embedded in aggregates with the goal of investigating the aggregate shear bands and geogrid deformation during pullout tests. The DEM models were initially calibrated using experimental pullout test results. The DEM simulations facilitated the visualization of the shear bands and geogrid deformation patterns. The following conclusions were drawn:

(1) Shear bands – zones of intense shear deformation due to strain localization – with distinct thicknesses developed above and below the geogrid reinforcement plane. The upper shear band above the geogrid was slightly thicker ($3.4D_{50}$) compared to the lower shear band ($2.3D_{50}$), which can be attributed to upward particle dilation at the geogrid-aggregate interface.

(2) The strain profiles showed a general decrease along the longitudinal rib length, with significant fluctuations at the intersections of transverse and longitudinal ribs. Bending deformation of transverse ribs at these junctions led to increased stress and strain at the edges, while the middle of the longitudinal ribs experienced smaller strains. Improving junction designs or materials could reduce these localized strain concentrations and enhance load distribution.

(3) Relevant bending deformations of the transverse ribs were observed, especially toward the frontal load application, which became more prominent with increasing pullout displacements. This highlights the need for geogrid materials that balance rigidity and flexibility to better accommodate deformation and enhance performance.

REFERENCES

Cundall, P.A., Strack, O.D.L., 1979. A discrete numerical model for granular assemblies. Geotechnique 29, 47-65.

Ferellec, J.-F., McDowell, G.R., 2010. A method to model realistic particle shape and inertia in DEM. Granular Matter 12, 459-467.

Ferellec, J.F., McDowell, G.R., 2012. Modelling of ballast-geogrid interaction using the discrete-element method. Geosynthetics International 19, 470-479.

Indraratna, B., Ngo, N.T., Rujikiatkamjorn, C., 2013. Deformation of coal fouled ballast stabilized with geogrid under cyclic load. Journal of Geotechnical and Geoenvironmental Engineering 139, 1275-1289.

Jewell, R.A., 1990. Reinforcement bond capacity. Geotechnique 40, 513-518.

Jewell, R.A., Milligan, G.W.E., Sarsby, R.W., Dubois, D., 1985. Interaction between soil and geogrids. Proc., Conference on Polymer Grid Reinforcement, London, pp.18-29.

Jia, Y., Zhang, J., Chen, X., Miao, C., Zheng, Y., 2023. DEM study on shear behavior of geogrid-soil interfaces subjected to shear in different directions. Computers and Geotechnics 156.

Jia, Y., Zhang, J., Ngo, T., Zheng, Y., 2024. Shear resistance evolution of geogrid-aggregate interfaces under direct shear: insights from 3D DEM simulations. Canadian Geotechnical Journal.

Jing, X.-Y., Zhou, W.-H., Zhu, H.-X., Yin, Z.-Y., Li, Y., 2018. Analysis of soil-structural interface behavior using three-dimensional DEM simulations. International Journal for Numerical and Analytical Methods in Geomechanics 42, 339-357.

Moraci, N., Recalcati, P., 2006. Factors affecting the pullout behaviour of extruded geogrids embedded in a compacted granular soil. Geotextiles and Geomembranes 24, 220-242.

Peng, X., Zornberg, J.G., 2019. Evaluation of soil-geogrid interaction using transparent soil with laser illumination. Geosynthetics International 26, 206-221.

Potyondy, D.O., Cundall, P.A., 2004. A bonded-particle model for rock. International Journal of Rock Mechanics and Mining Sciences 41, 1329-1364.

Stahl, M., Konietzky, H., te Kamp, L., Jas, H., 2014. Discrete element simulation of geogrid-stabilised soil. Acta Geotechnica 9, 1073-1084.

Wang, Y.-Q., Feng, S.-J., Zhao, Y., Zheng, Q.-T., 2024. Microscale analysis of geogrid–aggregate interface cyclic shear behavior using DEM. Computers and Geotechnics 166, 105973.

Zhou, J., Chen, J.F., Xue, J.F., Wang, J.Q., 2012. Micro-mechanism of the interaction between sand and geogrid transverse ribs. Geosynthetics International 19, 426-437.

Zornberg, J.G., Sitar, N., Mitchell, J.K., 2000. Performance of geosynthetic reinforced slopes at failure. Journal of Geotechnical Geoenvironmental Engineering 124, 670-683.